Cancer Research

Cis-Acting *circ-CTNNB1* Promotes β-Catenin Signaling and Cancer Progression via DDX3-Mediated Transactivation of YY1

Feng Yang[1], Erhu Fang[1], Hong Mei[1], Yajun Chen[2], Huanhuan Li[1], Dan Li[1], Huajie Song[1], Jianqun Wang[1], Mei Hong[1], Wenjing Xiao[2], Xiaojing Wang[3], Kai Huang[3], Liduan Zheng[2,3], and Qiangsong Tong[1,3]

Abstract

Circular RNAs (circRNA), a subclass of noncoding RNA characterized by covalently closed continuous loops, play emerging roles in tumorigenesis and aggressiveness. However, the functions and underlying mechanisms of circRNA in regulating Wnt/β-catenin signaling and cancer progression remain elusive. Here, we screen *cis*-acting circRNA generated by β-catenin (*CTNNB1*)/transcription factor 7–like 2 genes and identify one intronic circRNA derived from *CTNNB1* (*circ-CTNNB1*) as a novel driver of cancer progression. *Circ-CTNNB1* was predominantly expressed in the nucleus, upregulated in cancer tissues and cell lines, and associated with unfavorable outcomes in patients with cancer. *Circ-CTNNB1* promoted β-catenin activation, growth, invasion, and metastasis in cancer cells. *Circ-CTNNB1* bound DEAD-box polypeptide 3 (DDX3) to facilitate its physical interaction with transcription factor Yin Yang 1 (YY1), resulting in the transactivation of YY1 and transcriptional alteration of downstream genes associated with β-catenin activation and cancer progression. Preclinically, administration of lentivirus-mediated short hairpin RNA targeting *circ-CTNNB1* or a cell-penetrating inhibitory peptide blocking the *circ-CTNNB1*–DDX3 interaction inhibited downstream gene expression, tumorigenesis, and aggressiveness in cancer cells. Taken together, these results demonstrate *cis*-acting *circ-CTNNB1* as a mediator of β-catenin signaling and cancer progression through DDX3-mediated transactivation of YY1.

Significance: These findings reveal the oncogenic functions of a *cis*-acting circular RNA in β-catenin activation and cancer progression, with potential value as a therapeutic target for human cancers.

Introduction

The Wnt/β-catenin signaling pathway plays essential roles in biological processes, including embryogenesis, tissue homeostasis, and proliferation or differentiation of mammalian cells (1). Within the cytoplasm, β-catenin is constitutively phosphorylated at serine (Ser)/threonine (Thr) residues by glycogen synthase kinase 3 beta (GSK-3β), and phosphorylated β-catenin is degraded by the ubiquitin/proteasome pathway (2). Upon Wnt signals (such as WNT3), the phosphorylation of β-catenin is reduced, resulting in protein stabilization, cytoplasmic accumulation, and subsequent nuclear translocation, whereas it interacts with T-cell factor (TCF)/lymphoid enhancer-binding factor to modulate target gene expression (2). As characterized by nuclear β-catenin accumulation, activation of Wnt/β-catenin signaling is documented in many types of cancer and contributes to cancer progression (3, 4). However, the mechanisms underlying β-catenin activation in cancers still remain to be determined.

Circular RNAs (circRNA), a group of transcripts characterized by covalently closed continuous loops, are generated from exons or introns of parent genes (5). Exonic circRNAs are predominantly localized within the cytoplasm (6), and some of them (such as *ciRS-7* and *circSry*) regulate the expression of other genes *in trans* by serving as sponges for microRNA (miRNA; refs. 7, 8). Besides the *trans*-regulatory mode, circRNAs are able to regulate gene expression in a *cis*-acting manner. For example, circRNA derived from the second exon of muscleblind (*circMbl*) regulates parent gene expression by competing with linear splicing (9). Exonic circRNA generated from poly(A) binding protein nuclear 1 (*circPABPN1*) represses the translation of *PABPN1* via preventing the enrichment of human antigen R on mRNA (10). In addition, *ci-ankrd52*, originating from the intron of ankyrin repeat domain 52 (*ANKRD52*), binds RNA polymerase II to regulate the transcription of *ANKRD52* (11). A special class of exon–intron circRNAs is abundant in the nucleus, lacks miRNA binding sites, and is involved in transcriptional regulation of parent gene expression (12). Dysregulated circRNAs have been identified in almost all types of cancers, such as hepatocellular carcinoma,

[1]Department of Pediatric Surgery, Union Hospital, Tongji Medical College, Huazhong University of Science and Technology, Wuhan, Hubei Province, P. R. China. [2]Department of Pathology, Union Hospital, Tongji Medical College, Huazhong University of Science and Technology, Wuhan, Hubei Province, P. R. China. [3]Clinical Center of Human Genomic Research, Union Hospital, Tongji Medical College, Huazhong University of Science and Technology, Wuhan, Hubei Province, P. R. China.

Note: Supplementary data for this article are available at Cancer Research Online (http://cancerres.aacrjournals.org/).

F. Yang and E. Fang contributed equally to this article.

Corresponding Authors: Qiangsong Tong, Union Hospital, Tongji Medical College, Huazhong University of Science and Technology, 1277 Jiefang Avenue, Wuhan 430022, Hubei Province, P. R. China. Phone: 86-27-85350762; Fax: 86-27-85726821; E-mail: qs_tong@hotmail.com; and Liduan Zheng, Phone: 86-27-85726129; Fax: 86-27-85726821; E-mail: ld_zheng@hotmail.com

doi: 10.1158/0008-5472.CAN-18-1559

prostate cancer, and colorectal cancer (13). However, the roles of *cis*-acting circRNA in β-catenin activation and cancer progression still remain elusive.

In this study, through screening *cis*-regulatory circRNAs derived from β-catenin (*CTNNB1*) and transcription factor 7 like 2 (*TCF7L2*) genes, essential components of β-catenin/TCF transcriptional complexes (14), we identified one intronic circRNA derived from *CTNNB1* (*circ-CTNNB1*) as a driver of cancer progression. We demonstrate that *circ-CTNNB1* is upregulated in cancer tissues and facilitates the β-catenin activation, tumorigenesis, and aggressiveness. Mechanistically, *circ-CTNNB1* binds DEAD-box polypeptide 3 (DDX3) to facilitate its physical interaction with Yin Yang 1 (YY1), which results in transactivation of YY1 and subsequent transcriptional alteration of downstream genes associated with β-catenin activation, indicating the essential roles of the *circ-CTNNB1*/DDX3/YY1 axis in cancer progression.

Materials and Methods

Cell culture

Human embryonic kidney (HEK293T) cells and cell lines of gastric cancer (MKN-45 and AGS), cervical cancer (HeLa), prostate cancer (PC-3), breast cancer (MCF-7), colon cancer (HCT-116 and LoVo), liver cancer (HepG2), and neuroblastoma [BE(2)-C and SH-SY5Y] were obtained from American Type Culture Collection and Japanese Collection of Research Bioresources Cell Bank, authenticated by short tandem repeat profiling, and used within 6 months after resuscitation of frozen aliquots. *Mycoplasma* contamination was regularly examined using the Lookout Mycoplasma PCR Detection Kit (Sigma). Cells were cultured with RPMI1640 containing 10% fetal bovine serum (Life Technologies, Inc.), incubated in serum-free RPMI-1640 for 4 hours, and treated with XAV939 (Selleckchem), WNT3a (R&D Systems, Inc.), or lithium chloride (LiCl, Sigma).

RT-PCR and real-time quantitative RT-PCR

Nuclear, cytoplasmic, and total RNAs were extracted using the RNA Subcellular Isolation Kit (Active Motif) or RNeasy Mini Kit (Qiagen Inc.). For circRNA detection, RNase R (3 U/mg, Epicenter) digestion was undertaken at 37°C for 15 minutes. Reverse transcription and real-time PCR were performed using the Transcriptor First Strand cDNA Synthesis Kit (Roche), SYBR Green PCR Master Mix (Applied Biosystems), and primer sets (Supplementary Table S1). The results of transcript levels were analyzed by the $2^{-\Delta\Delta Ct}$ method.

Northern blot

The junction or nonjunction probe for *circ-CTNNB1* was synthesized and labeled by digoxigenin (DIG; Supplementary Table S2). Northern blot was performed as previously described (7, 8). Blots were washed stringently, detected by anti-DIG antibody, and recorded on X-ray films with chemiluminescence substrate CSPD (Roche).

Western blot

Tissue or cellular protein was extracted with 1 × cell lysis buffer (Promega). Western blot was performed as previously described (15, 16), with antibodies specific for β-catenin (ab32572), c-myc (ab32072), cyclin D1 (ab134175), DDX3 (ab37160), RNA-binding motif protein 14 (RBM14, ab70636), RNA-binding motif protein 39 (RBM39, ab12326), YY1 (ab109228), Wnt family member 1 (WNT1, ab15251), WNT3 (ab172612), axin 2 (AXIN2, ab109307), frizzled class receptor 10 (FZD10, ab83044), bone morphogenetic protein 4 (BMP4, ab39973), FLAG (ab1162), Myc (ab9106), β-actin (ab8226, Abcam Inc.), phosphorylated β-catenin (Ser33/Ser37, sc-57535), glutathione S-transferase (GST, sc-33614), histone H3 (sc-24516), and glyceraldehyde 3-phosphate dehydrogenase (GAPDH, sc-47724, Santa Cruz Biotechnology).

Overexpression or knockdown of genes

Linear *circ-CTNNB1* (378 bp) was obtained from gastric cancer tissues by PCR (Supplementary Table S2) and inserted into pLCDH-ciR (Geenseed Biotech Co.). Human *DDX3* cDNA (1989 bp) and its Myc-tagged truncations were provided by Dr. Christof Niehrs (Institute of Molecular Biology, Mainz, Germany), whereas *YY1* cDNA (1,245 bp) was a gift from Dr. Makoto Miyagishi (National Institute of Advanced Industrial Science and Technology, Tokyo, Japan). The amplified truncations of *DDX3* and *YY1* (Supplementary Table S2) were subcloned into pGEX-6P-1 or pCMV-3Tag-1A (Addgene). Mutation of *DDX3* was prepared with GeneTailor Site-Directed Mutagenesis System (Invitrogen) and PCR primers (Supplementary Table S2). Oligonucleotides encoding short hairpin RNA (shRNA) against *circRNAs, DDX3*, *YY1*, ETS-related gene (*ERG*), or specificity protein 1 (*SP1*; Supplementary Table S3) were inserted into GV298 (GeneChem Co., Ltd). After selection for neomycin or puromycin (Invitrogen) resistance, stable cell lines were obtained.

Lentiviral vector construction

Lentiviral vectors were cotransfected with packaging plasmids psPAX2 and pMD2G into HEK293T cells. Infectious lentiviruses were harvested at 36 and 60 hours after transfection and filtered through 0.45-μm PVDF filters. Recombinant lentiviruses were concentrated 100-fold by ultracentrifugation (2 hours at 120,000 × *g*).

RNA sequencing assay

Total RNA was extracted using TRIzol reagent (Life Technologies, Inc.). Transcriptome sequencing on an Illumina HiSeq X Ten platform was carried out at Novogene Bioinformatics Technology Co., Ltd. Sequencing results were deposited in the Gene-Expression Omnibus database (accession code GSE120496).

Dual-luciferase reporter assay

The TOP-FLASH and FOP-FLASH reporters were obtained from Millipore. Human *YY1* luciferase reporter was established by inserting complementary oligonucleotides containing four canonical YY1 binding sites (Supplementary Table S2) into pGL3-Basic (Promega). Dual-luciferase assay was performed as previously described (15, 16). Relative β-catenin activation was determined by the TOP-FLASH/FOP-FLASH ratio.

Biotin-labeled RNA pulldown and mass spectrometry analysis

The 5′-monophosphorylated linear or random probe of *circ-CTNNB1* was *in vitro* transcribed using Biotin RNA Labeling Mix (Roche), reaction mixture containing excessive guanosine monophosphate (7.5 mmol/L) and guanosine triphosphate (1.5 mmol/L), and T7 RNA polymerase (17, 18). After incubation with guide oligonucleotide targeting circular junction (Supplementary Table S2), the 5′-monophosphorylated linear probe was circularized using T4 RNA ligase I, treated with RNase R, and purified with RNeasy Mini Kit (Qiagen Inc.). The lysates of 2×10^7 cancer cells were incubated with 3 μg of biotin-labeled probe, and

treated with 35 μL of Streptavidin C1 magnetic beads (Invitrogen) for 1 hour. The retrieved protein was detected by Western blot or mass spectrometry analysis (Wuhan Institute of Biotechnology; ref. 15).

RNA fluorescence *in situ* hybridization

Cells were seeded on coverslips, fixed with 4% paraformaldehyde, and incubated with 50% formamide, 2 × SSC, *E. coli* transfer RNA (0.25 mg/mL), salmon sperm DNA (0.25 mg/mL; Life Technologies, Inc.), bovine serum albumin (2.5 mg/mL; Roche), and DIG-labeled antisense or sense probe for *circ-CTNNB1* junction (Supplementary Table S2). The probes for *GAPDH* and *U1* were generated by *in vitro* transcription of PCR products (Supplementary Table S1) using DIG Labeling Kit (MyLab Corporation). Hybridization was undertaken using the Fluorescent *In Situ* Hybridization Kit (RiboBio), with or without RNase R (3 U/mg) treatment, whereas nuclei were counterstained using 4′,6-diamidino-2-phenylindole (DAPI).

Fluorescence immunocytochemical staining

Cancer cells were grown on coverslips, and incubated with antibodies specific for β-catenin (ab32572; Abcam Inc.; 1:100 dilution) or DDX3 (ab37160; Abcam Inc.; 1:100 dilution). Then, coverslips were treated with Alexa Fluor 594 or 498 goat anti-rabbit IgG (1:1,000 dilution) and DAPI (300 nmol/L) staining.

Coimmunoprecipitation assay

Coimmunoprecipitation was undertaken as previously described (15), with antibodies specific for DDX3 (sc-365768; Santa Cruz Biotechnology), YY1 (ab109228), FLAG (ab1162), or Myc (ab9106, Abcam Inc.).

Bimolecular fluorescence complementation assay

Human *DDX3* cDNA (1989 bp) and *YY1* cDNA (1,245 bp) were subcloned into bimolecular fluorescence complementation (BiFC) vectors pBiFC-VN173 and pBiFC-VC155 (Addgene), respectively (Supplementary Table S2). The recombinant constructs were cotransfected into cancer cells for 24 hours. The fluorescence emission was observed under a confocal microscope, with excitation and emission wavelengths of 488 and 500 nm, respectively.

Rescue of target gene expression

To rescue the *circ-CTNNB1* knockdown-altered levels of target genes, the expression vector of *DDX3* or *YY1* was transfected into stable cell lines. To restore the altered expression of target genes induced by *circ-CTNNB1*, shRNAs against *DDX3* or *YY1* (Supplementary Table S3) were transfected into cancer cells using Genesilencer Transfection Reagent (Genlantis).

Chromatin immunoprecipitation

Chromatin immunoprecipitation (ChIP) assay was undertaken using EZ-ChIP kit (Upstate Biotechnology; refs. 15, 16), with antibodies specific for YY1 (ab38422), enhancer of zeste homolog 2 (EZH2, ab228697), histone deacetylase 1 (HDAC1, ab7028), or p300 (ab14984, Abcam Inc.) and primer sets (Supplementary Table S1).

Cross-linking RNA immunoprecipitation assay

Cells were cross-linked by ultraviolet light at 254 nm (200 J/cm^2; refs. 15, 16). RNA immunoprecipitation (RIP) assay was performed using Magna RIP RNA Binding Protein Immunoprecipitation Kit (Millipore), using antibodies specific for DDX3 (sc-365768, Santa Cruz Biotechnology) or FLAG (ab1162, Abcam Inc.). Coprecipitated RNAs were detected by RT-PCR or real-time quantitative RT-PCR (qRT-PCR) with primers (Supplementary Table S1).

***In vitro* binding assay**

A series of *DDX3* truncates were amplified with primer sets (Supplementary Table S2), subcloned into pGEX-6P-1 (Addgene), and transformed into *E. coli* to produce GST-tagged DDX3 truncation proteins (15, 16). The DDX3–circRNA complexes were pulled down using GST beads (Sigma). Protein was detected by SDS-PAGE and Western blot, whereas circRNA was measured by RT-PCR with divergent primers (Supplementary Table S1).

RNA electrophoretic mobility shift assay

Biotin-labeled *circ-CTNNB1* probe was prepared as described above. RNA electrophoretic mobility shift assay (EMSA) using nuclear extracts or recombinant DDX3 protein was performed using LightShift Chemiluminescent RNA EMSA Kit (Thermo Fisher Scientific, Inc.).

Design and synthesis of inhibitory peptides

The inhibitory peptides blocking the *circ-CTNNB1*-DDX3 interaction were designed, and chemically synthesized by linking with biotin-labeled cell-penetrating peptide (YGRKKRRQRRR) from Tat protein transduction domain at the N-terminus and conjugating with fluorescein isothiocyanate (FITC) at the C-terminus (ChinaPeptides Co. Ltd), with purity larger than 95%.

Biotin-labeled peptide pulldown assay

Cellular total RNA was isolated using the RNeasy Mini Kit (Qiagen Inc.) and incubated with biotin-labeled peptide and streptavidin-agarose at 4°C. The beads were extensively washed, and circRNA pulled down was measured by RT-PCR or real-time qRT-PCR.

***In vitro* cell viability, growth, and invasion assays**

The 2-(4,5-dimethyltriazol-2-yl)-2,5-diphenyl tetrazolium bromide (MTT, Sigma) colorimetric (15), soft agar (15, 16), and Matrigel invasion (15, 16) assays were undertaken to measure the *in vitro* viability, growth, and invasiveness of cancer cells.

***In vivo* growth, metastasis, and therapeutic assays**

All animal experiments were carried out in accordance with NIH Guidelines for the Care and Use of Laboratory Animals and approved by the Animal Care Committee of Tongji Medical College (approval number: Y20080290). The *in vivo* tumor growth (1×10^6 cancer cells per mouse, $n = 5$ per group) and experimental metastasis (0.4×10^6 cancer cells per mouse, $n = 5$ per group) studies were performed with blindly randomized 4-week-old female BALB/c nude mice as previously described (15, 16). For *in vivo* therapeutic studies, after cancer cell inoculation, mice were blindly randomized and treated by intratumoral or tail-vein injection of lentivirus-mediated shRNA (1×10^7 plaque-forming units) or synthesized cell-penetrating peptide (ChinaPeptides) as indicated. The *In Vivo* Optical Imaging System (*In Vivo* FX PRO, Bruker Corporation) was applied to acquire fluorescent images of xenografts in nude mice.

Patient tissue samples

Human tissue study was approved by the Institutional Review Board of Tongji Medical College (approval number: 2011-S085). All procedures were undertaken in accordance with guidelines set forth by the Declaration of Helsinki. Written informed consent was obtained from all patients. Fresh cancer tissues were collected at surgery, validated by pathologic diagnosis, and stored at −80°C.

IHC

IHC staining and quantitative evaluation were performed as previously described (15, 16), with antibodies specific for Ki-67 (sc-23900, Santa Cruz Biotechnology) or CD31 (ARG52748, Arigo).

Statistical analysis

All data were shown as mean ± SEM. The cutoff for gene expression was defined by average values. Student *t* test, analysis of variance, and χ^2 analysis were used to compare the difference in cancer cells or tissues. Fisher exact test was used to analyze the overlapping of genes. Pearson correlation coefficient assay was used to analyze the expression correlation. Log-rank test was used to assess survival difference. All statistical tests were two-sided.

Results

circ-CTNNB1 is a *cis*-acting circRNA upregulated in cancer tissues and cells

Mining of the circRNA databases circBase (19) and circInteractome (20) revealed 38 potential *cis*-acting circRNAs derived from the *CTNNB1* and *TCF7L2* genes, with 15 having more than 2 read scores (Fig. 1A). Further validating RT-PCR with divergent primers revealed 7 detectable circRNAs in gastric cancer AGS cells (Supplementary Fig. S1A). Three circRNAs, *hsa_circ_0020050*, *hsa_circ_0004030*, and *hsa_circ_0123778* (*circ-CTNNB1*), were upregulated in the tissues of gastric cancer, prostate cancer, and colorectal cancer (Fig. 1B; Supplementary Fig. S1B), cancer types with obvious β-catenin activation (3, 4, 21). Knockdown of *circ-CTNNB1*, but not of *hsa_circ_0020050* or *hsa_circ_0004030*, attenuated the β-catenin activity in gastric cancer AGS and colon cancer HCT-116 cells, with similar effects to the established β-catenin inhibitor XAV939 (Fig. 1C; Supplementary Fig. S1C; ref. 22). The existence of 378-nt *circ-CTNNB1* generated from intron 10 of *CTNNB1* (Fig. 1D) was further confirmed by RT-PCR with divergent primers and Sanger sequencing (Fig. 1E). Endogenous or ectopic expression of *circ-CTNNB1* resistant to RNase R digestion was also detected by a junction-specific probe in Northern blot (Fig. 1F), which did not detect the pre-mRNA or mRNA bands of *CTNNB1* (Fig. 1F). Higher *circ-CTNNB1* levels were observed in cancer cell lines than those of embryonic kidney HEK293T cells (Fig. 1G). In addition, *circ-CTNNB1* was elevated in gastric cancer tissues with metastasis than those without metastasis ($P < 1.0 \times 10^{-4}$; Fig. 1H). Kaplan–Meier survival analysis of 81 gastric cancer cases indicated that high *circ-CTNNB1* expression was associated with poor overall survival of patients ($P < 1.0 \times 10^{-4}$; Fig. 1I). These results indicated that *circ-CTNNB1* was a *cis*-acting circRNA upregulated in cancer tissues and cells.

Circ-CTNNB1 promotes the growth and aggressiveness of cancer cells

To explore the roles of *circ-CTNNB1* in cancer progression, cancer cell lines representing moderate expression levels were applied. The *circ-CTNNB1* vector–induced circularization efficiency was approximately 80% in Northern blot (Supplementary Fig. S2A). Stable transfection of *circ-CTNNB1* and three independent shRNAs against *circ-CTNNB1* (sh-circ-CTNNB1) into gastric cancer cell lines MKN-45 and AGS, prostate cancer PC-3 cells, and colon cancer HCT-116 cells resulted in increased and reduced levels of *circ-CTNNB1*, respectively (Supplementary Fig. S2B), which were resistant to efficient RNase R digestion (Supplementary Fig. S2C). Stable overexpression or knockdown of *circ-CTNNB1* facilitated and reduced the viability, anchorage-independent growth and invasiveness of cancer cells, respectively (Fig. 2A–C; Supplementary Fig. S2D and S2E). Consistently, stable transfection of *circ-CTNNB1* or sh-circ-CTNNB1 #3 resulted in a significant increase and decrease in the growth, tumor weight, Ki-67 proliferation index, and CD31-positive intratumoral microvessels of MKN-45 cell–formed subcutaneous xenografts, respectively (Fig. 2D and E). In experimental metastasis assay, athymic nude mice treated with tail-vein injection of MKN-45 cells stably transfected with *circ-CTNNB1* or sh-circ-CTNNB1 #3 displayed more and fewer lung metastatic colonies, with lower and greater survival probability, respectively (Fig. 2F and G). These results suggested that *circ-CTNNB1* promoted the growth and aggressiveness of cancer cells *in vivo* and *in vitro*.

Circ-CTNNB1 increases the expression of β-catenin in cancer cells

To elucidate the mechanisms underlying the oncogenic roles of *circ-CTNNB1*, we investigated its effects on the expression of its parent gene *CTNNB1*. Stable transfection of *circ-CTNNB1* or sh-circ-CTNNB1 #3 increased and decreased the protein levels, but not the promoter activity or transcript levels, of *CTNNB1* in MKN-45, AGS, PC-3, and HCT-116 cells (Fig. 3A–C; Supplementary Fig. S3A and Supplementary Fig. S3B). Increased cytoplasmic and nuclear accumulation of β-catenin was observed in MKN-45 and AGS cells stably overexpressing *circ-CTNNB1* (Fig. 3D and E; Supplementary Fig. S3C). In addition, stable transfection of *circ-CTNNB1* or sh-circ-CTNNB1 #3 resulted in increased and decreased β-catenin activity, and abolished the effects of Wnt signaling inhibitor (XAV939) and activator (WNT3a) in cancer cells, respectively (Fig. 3F). To determine whether *circ-CTNNB1* affected the degradation of β-catenin, we observed the alteration in phosphorylated β-catenin levels in cancer cells. Ectopic expression of *circ-CTNNB1* decreased the phosphorylation of β-catenin and increased the expression of β-catenin and its downstream genes *c-Myc* and *cyclin D1* (Fig. 3G). Meanwhile, knockdown of *circ-CTNNB1* led to increased phosphorylation of β-catenin and decreased β-catenin levels (Fig. 3H), which was rescued by treatment of cancer cells with WNT3a or GSK-3β inhibitor LiCl (Fig. 3H). In addition, treatment with a proteasome inhibitor (MG-132) abolished the decrease in β-catenin expression induced by knockdown of *circ-CTNNB1* (Fig. 3H). These findings indicated that *circ-CTNNB1* increased the expression of β-catenin in cancer cells.

Circ-CTNNB1 is predominantly localized in the nucleus and interacts with DDX3

We further investigated the localization and protein partners of *circ-CTNNB1* within cancer cells. RNA fluorescence *in situ* hybridization (RNA-FISH) and subcellular fractionation assays revealed abundant signals and enrichment of *circ-CTNNB1* in the nucleus (Fig. 4A and B). To identify the protein partner of *circ-CTNNB1*, we

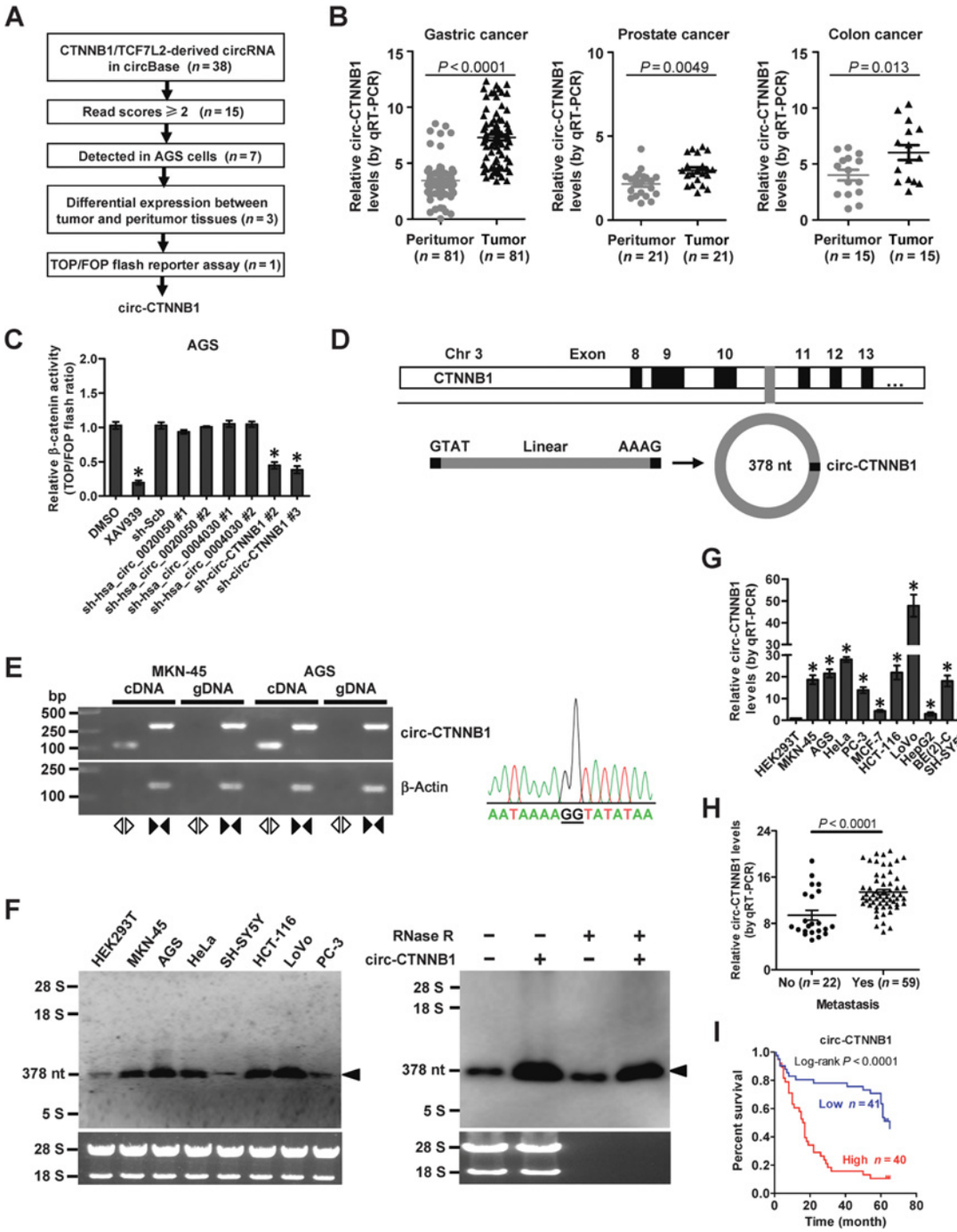

Figure 1.

Identification of *circ-CTNNB1* as a *cis*-acting circRNA upregulated in cancer tissues and cells. **A,** Flowchart delineating the identification of *circ-CTNNB1* as a *cis*-acting circRNA regulating β-catenin activity. **B,** Real-time qRT-PCR assay showing the relative levels of *circ-CTNNB1* (normalized to β-actin) in the peritumor and tumor tissues of gastric cancer ($n = 81$), prostate cancer ($n = 21$), and colon cancer ($n = 15$). **C,** TOP/FOP flash assay indicating the β-catenin activity in AGS cells transfected with scramble shRNA (sh-Scb) or shRNA specific for circRNAs and in those treated with solvent control (DMSO) or XAV939 (5.0 μmol/L) for 6 hours. **D,** Schematic illustration showing the genomic location of *circ-CTNNB1* derived from its parent gene *CTNNB1*. **E,** RT-PCR or PCR assay (left) indicating the detection of *circ-CTNNB1* using divergent and convergent primers from cDNA or genomic DNA (gDNA) of cancer cells, with further validation by Sanger sequencing (right). **F,** Northern blot using a junction-specific probe showing the endogenous existence of *circ-CTNNB1* in HEK293T cells and cancer cell lines (left), and that of AGS cells transfected by *circ-CTNNB1* and treated with RNase R (3 U/mg, right). **G,** Real-time qRT-PCR assay revealing the relative levels of *circ-CTNNB1* (normalized to β-actin) in HEK293T and cancer cell lines (mean ± SEM; $n = 4$). **H,** Real-time qRT-PCR assay showing the levels of *circ-CTNNB1* (normalized to β-actin) in gastric cancer tissues with differential status of metastasis. **I,** Kaplan–Meier curves indicating overall survival of 81 patients with gastric cancer with low or high expression of *circ-CTNNB1* (cutoff value = 12.14). *, $P < 0.01$ vs. DMSO, sh-Scb, or HEK293T. Student *t* test compared gene-expression levels in **B**, **C**, **G,** and **H**. Log-rank test for survival comparison in **I**.

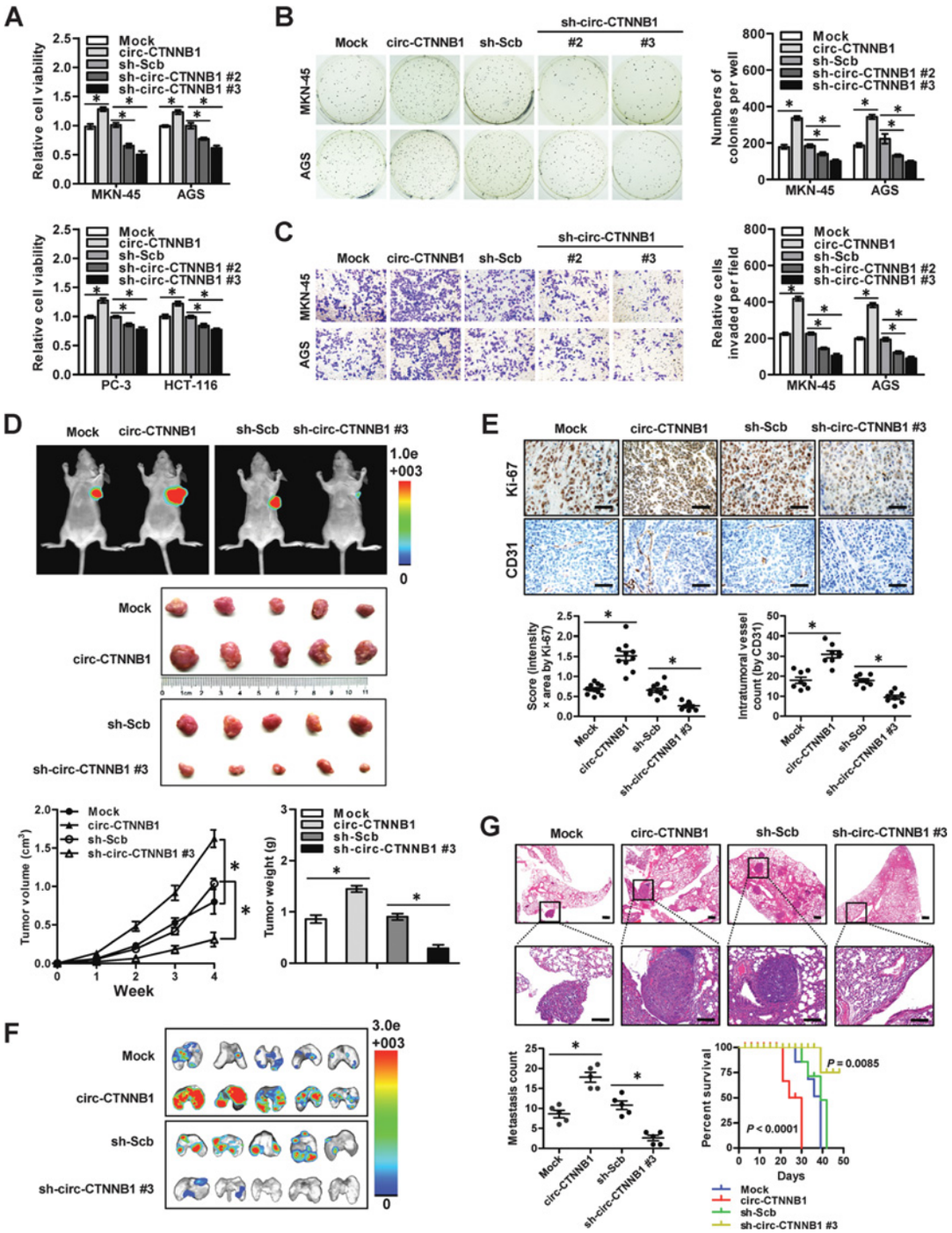

Figure 2.

Circ-CTNNB1 promotes the growth and aggressiveness of cancer cells *in vitro* and *in vivo*. **A,** MTT colorimetric assay showing the viability of MKN-45, AGS, PC-3, and HCT-116 cells stably transfected with empty vector (mock), *circ-CTNNB1*, scramble shRNA (sh-Scb), or sh-circ-CTNNB1. **B** and **C,** Representative images (left) and quantification (right) of soft-agar (**B**) and Matrigel invasion (**C**) assays indicating the anchorage-independent growth and invasion of MKN-45 and AGS cells stably transfected with mock, *circ-CTNNB1*, sh-Scb, or sh-circ-CTNNB1. **D,** Representative images (top and middle), *in vivo* growth curve (bottom left), and weight at the end points (bottom right) of xenografts formed by subcutaneous injection of MKN-45 cells stably transfected with mock, *circ-CTNNB1*, sh-Scb, or sh-circ-CTNNB1 #3 into the dorsal flanks of nude mice ($n = 5$ for each group). **E,** Representative images (top) and quantification (bottom) of IHC staining showing the intratumoral expression of Ki-67 and CD31 within xenografts ($n = 5$ for each group). Scale bars, 50 μm. **F** and **G,** Representative images (**F**), hematoxylin and eosin staining (**G**, top), and quantification (**G**, bottom left) of lung metastatic colonization and Kaplan–Meier curves (**G**, bottom right) of nude mice treated with tail-vein injection of MKN-45 cells stably transfected with mock, *circ-CTNNB1*, sh-Scb, or sh-circ-CTNNB1 #3 ($n = 5$ for each group). Student *t* test and analysis of variance compared the difference in **A–E** and **G**. Log-rank test for survival comparison in **G**. *, $P < 0.01$ vs. mock or sh-Scb.

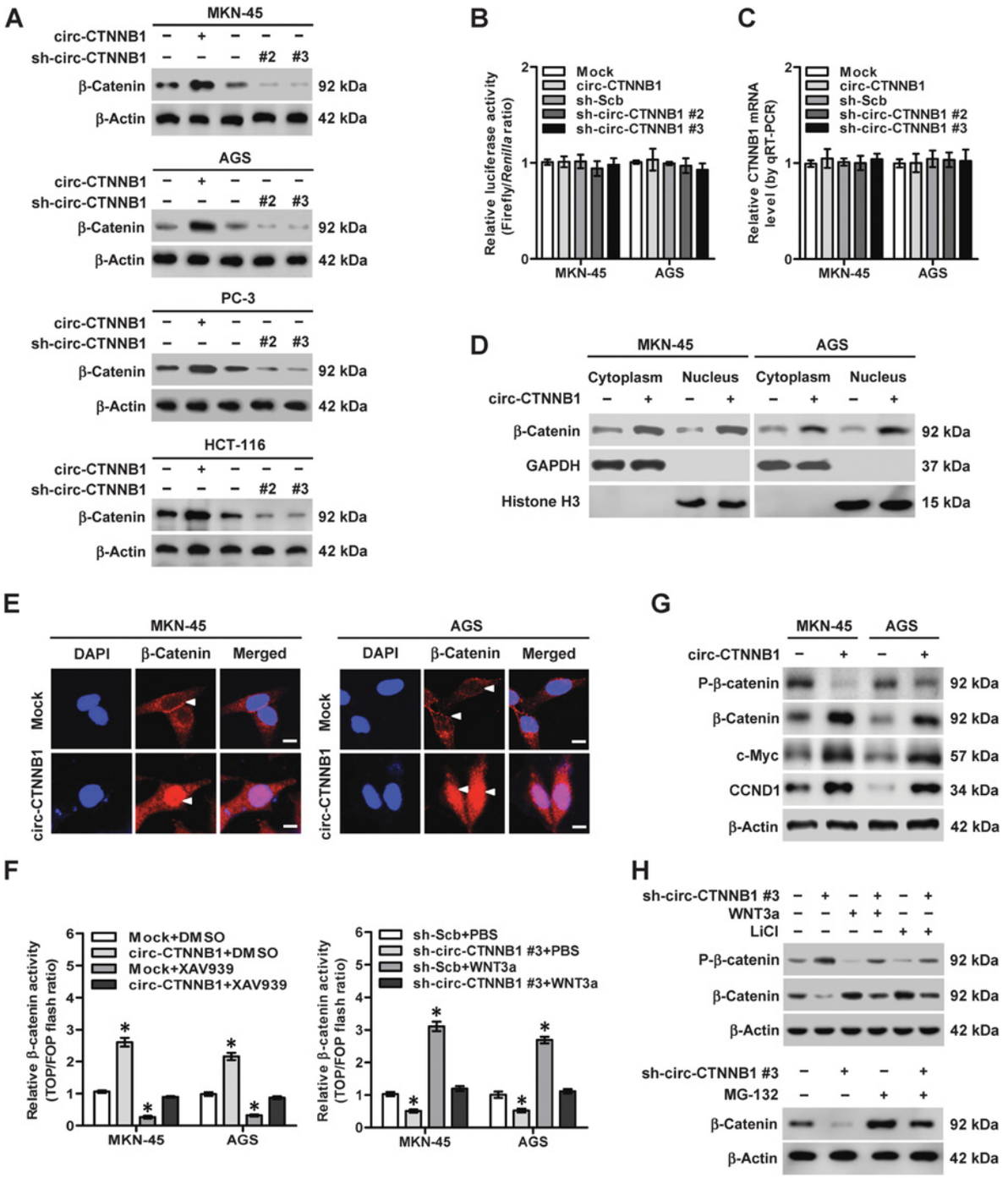

Figure 3.

Circ-CTNNB1 increases the expression of β-catenin in cancer cells. **A,** Western blot assay showing the protein levels of β-catenin in MKN-45, AGS, PC-3, and HCT-116 cells stably transfected with empty vector (mock), *circ-CTNNB1*, scramble shRNA (sh-Scb), or sh-circ-CTNNB1. **B** and **C,** Dual-luciferase (**B**) and real-time qRT-PCR (**C**) assays indicating the promoter activity and transcript levels of *β-catenin* in MKN-45 and AGS cells stably transfected with mock, *circ-CTNNB1*, sh-Scb, or sh-circ-CTNNB1 (mean ± SEM; $n = 4$). **D** and **E,** Western blot (**D**) and immunofluorescence (**E**) assays showing the cytoplasmic and nuclear accumulation of β-catenin in MKN-45 and AGS cells stably transfected with mock or *circ-CTNNB1*. Scale bar, 10 μm. **F,** Dual-luciferase assay indicating the activity of β-catenin in cancer cells stably transfected with mock, *circ-CTNNB1*, sh-Scb, or sh-circ-CTNNB1 #3, and those treated with solvent control (DMSO), XAV-939 (5.0 μmol/L), PBS, or WNT3a (50 ng/mL). **G,** Western blot showing the expression of phosphorylated β-catenin (Ser33/Ser37), β-catenin, c-myc, and cyclin D1 in cancer cells stably transfected with mock or *circ-CTNNB1*. **H,** Western blot indicating the expression of phosphorylated β-catenin (Ser33/Ser37) and β-catenin in MKN-45 cells stably transfected with sh-Scb or sh-circ-CTNNB1 #3, and those treated with WNT3a (50 ng/mL), LiCl (30 mmol/L), or proteasome inhibitor (MG132, 12.5 μmol/L). Student *t* test and analysis of variance compared the difference in **B**, **C**, and **F**. *, $P < 0.01$ vs. mock + DMSO or sh-Scb + PBS.

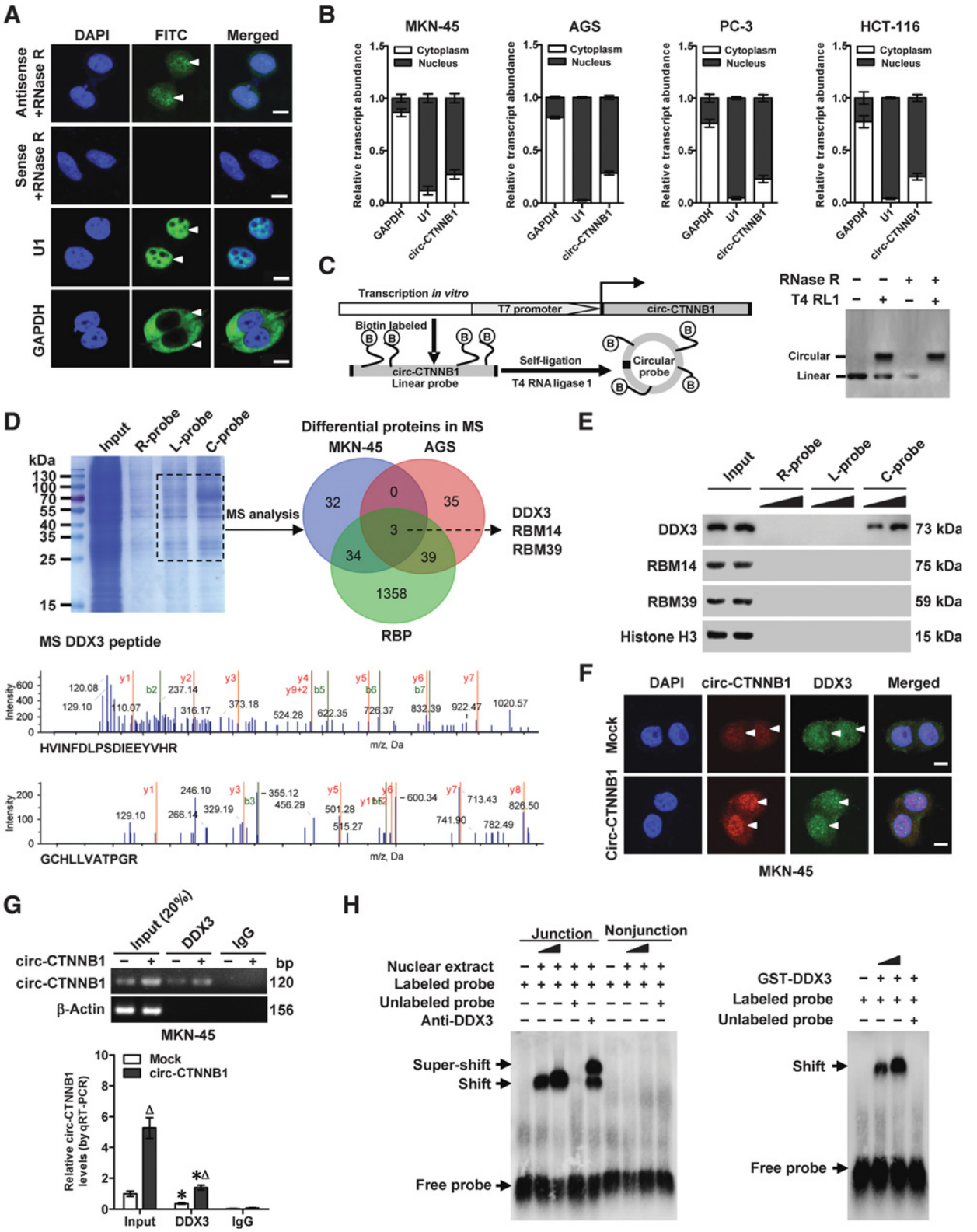

performed the biotin-labeled RNA pulldown followed by a proteomic analysis of RNA-associated protein complex in cancer cells, using the circRNA probe generated by ligation of *in vitro*–transcribed linear *circ-CTNNB1* (Fig. 4C; refs. 17, 18). Mass spectrometry assay revealed 69 and 77 differential proteins between *circ-CTNNB1* and linear transcript pulldown groups form MKN-45 and AGS cells, respectively (Fig. 4D; Supplementary Table S4), and overlapping with established RNA-binding proteins (RBP; //www.ablife.cc) indicated three RBPs consistently pulled down by biotin-labeled *circ-CTNNB1* in both cell lines (Fig. 4D), including DDX3, RBM14, and RBM39. Validating biotin-labeled RNA pulldown assay further indicated that *circ-CTNNB1* was able to dose dependently interact with DDX3, but not with RBM14 or RBM39, in the lysates of MKN-45 cells (Fig. 4E). However, no interaction was detected between DDX3 and linear or random probe (Fig. 4E). Dual RNA-FISH and immunofluorescence assay confirmed the colocalization of *circ-CTNNB1* and DDX3 in MKN-45 cells, which was increased by ectopic expression of *circ-CTNNB1* (Fig. 4F). RIP assay indicated the endogenous enrichment of *circ-CTNNB1* in RNA coprecipitated by DDX3 antibody in MKN-45 cells, which was increased by stable overexpression of *circ-CTNNB1* (Fig. 4G). Consistently, RNA EMSA showed that *circ-CTNNB1* strongly interacted with endogenous DDX3 in nuclear extracts or GST-tagged recombinant DDX3 protein (Fig. 4H). These findings indicated that *circ-CTNNB1* was predominantly localized in the nucleus and interacted with DDX3.

Circ-CTNNB1 cooperates with DDX3 to facilitate the expression and activity of β-catenin

We further investigated the interplay between *circ-CTNNB1* and DDX3 in regulating the expression and activity of β-catenin. Knockdown of *DDX3* or treatment with an established DDX3 inhibitor (RK-33; ref. 23) abolished the increased β-catenin expression induced by ectopic expression of *circ-CTNNB1* in MKN-45 cells (Fig. 5A; Supplementary Fig. S3D). Meanwhile, ectopic expression of *DDX3* prevented the decrease of β-catenin levels in MKN-45 and AGS cells with stable knockdown of *circ-CTNNB1* (Supplementary Fig. S3E). In addition, RK-33 treatment and *DDX3* overexpression abolished the increased and decreased β-catenin activity in MKN-45 and AGS cells stably transfected with *circ-CTNNB1* or sh-circ-CTNNB1 #3, respectively (Fig. 5B). *In vitro* binding assay indicated that RNA-binding domain [256-315 amino acids (aa)] of FLAG-tagged or GST-tagged DDX3 protein was crucial for its interaction with *circ-CTNNB1* (Fig. 5C). Mutation of amino acids (274–279, PTRELA) within Ia domain analyzed by RNABindRPlus (24) abolished the interaction of DDX3 with *circ-CTNNB1* (Fig. 5C). Notably, ectopic expression or knockdown of *DDX3* did not affect the *circ-CTNNB1* levels in MKN-45 and AGS cells (Fig. 5D), whereas the DDX3 protein levels were not affected by overexpression or knockdown of *circ-CTNNB1* (Fig. 5E). These results suggested that *circ-CTNNB1* cooperated with DDX3 to facilitate the expression and activity of β-catenin in cancer cells.

Circ-CTNNB1 facilitates DDX3-mediated transactivation of YY1 and target gene expression

To explore the downstream targets of *circ-CTNNB1*, we observed the *circ-CTNNB1*-induced differentially expressed genes by RNA-seq in AGS cells. There were 2,230 genes, including 1,244 upregulated and 986 downregulated ones, that showed differential expression (fold change >1.5, $P < 0.05$) upon *circ-CTNNB1* overexpression (Fig. 6A). Gene ontology analysis indicated that these *circ-CTNNB1* target genes were significantly associated with the Wnt signaling pathway, including *WNT1*, *WNT3*, *AXIN2*, *FZD10*, and *BMP4* (Fig. 6A). Comprehensive analysis using the ChIP-X program (25) and DDX3-interacting proteins derived from the BioGRID database (26) revealed three potential transcription factors regulating these target genes, including ERG (27), SP1 (28), and YY1 (Fig. 6B; Supplementary Table S5; ref. 29). Knockdown of *YY1*, but not of *ERG* or *SP1*, attenuated the increased β-catenin activity induced by stable *circ-CTNNB1* overexpression in MKN-45 and AGS cells (Fig. 6C; Supplementary Figs. S3D and S4A). Coimmunoprecipitation and BiFC (30) assays revealed endogenous interaction between DDX3 and YY1 in cancer cells, which was increased by ectopic expression of *circ-CTNNB1* (Fig. 6D and E). In addition, treatment with RK-33 attenuated the increased interaction between DDX3 and YY1 in MKN-45 cells stably transfected with *circ-CTNNB1* (Fig. 6D). The zinc finger (ZnF) domain (228–414 aa) or recruitment of polycomb (REPO) domain (205–226 aa), but not N-terminus (1–200 aa), of FLAG-tagged *YY1* was essential for its interaction with DDX3 protein (Supplementary Fig. S4B). Meanwhile, the V domain (425–456 aa) of Myc-tagged *DDX3* was essential for its interaction with YY1 (Supplementary Fig. S4B).

In dual-luciferase assay with a reporter containing four canonical YY1 binding sites, ectopic expression or knockdown of *circ-CTNNB1* prevented the decrease and increase of YY1 transactivation induced by silencing or overexpression of *DDX3* in cancer cells, respectively (Fig. 6F). Ectopic expression of *circ-CTNNB1* facilitated the interaction of YY1 with p300, and repressed its

Figure 4.

Circ-CTNNB1 is predominantly localized in the nucleus and interacts with DDX3. **A,** RNA-FISH assay showing the nuclear localization of *circ-CTNNB1* in MKN-45 cells incubated with a 58-bp junction antisense probe (green) and RNase R (3 U/mg), with the nuclei staining by DAPI (blue). Sense probe with RNase R (3 U/mg) treatment was used as a negative control. The *U1* and *GAPDH* were applied as positive controls. Scale bar, 10 μm. **B,** Real-time qRT-PCR indicating the distribution of *GAPDH, U1*, and *circ-CTNNB1* in the cytoplasmic and nuclear fractions (mean ± SEM; $n = 4$). **C,** Schematic diagram showing the process to generate biotin-labeled *circ-CTNNB1* probe by ligation of *in vitro* transcribed linear transcript (left), with validation by denaturing PAGE, SYBR Green II staining, and RNase R (3 U/mg) treatment (right). **D,** Coomassie bright blue staining (top left), Venn diagram (top right), and mass spectrometry (MS; bottom) assays revealing the proteins pulled down by biotin-labeled *circ-CTNNB1* from the lysates of MKN-45 and AGS cells, and their overlapping analysis with established RBP. **E,** Western blot assay showing the proteins pulled down by biotin-labeled random (R), linear (L), or circular (C) RNA probes from the lysates of MKN-45 cells. **F,** Dual RNA-FISH and immunofluorescence staining assay indicating the colocalization of *circ-CTNNB1* (red) and DDX3 (green) in MKN-45 cells stably transfected with empty vector (mock) or *circ-CTNNB1*, with nuclei staining with DAPI (blue). Scale bar, 10 μm. **G,** RIP (top) and real-time qRT-PCR (bottom) assays using an antibody specific for DDX3 showing the interaction between *circ-CTNNB1* and DDX3 in MKN-45 cells stably transfected with mock or *circ-CTNNB1*. **H,** RNA EMSA determining the interaction between endogenous (within nuclear extracts of MKN-45 cells) or recombinant DDX3 protein and biotin-labeled RNA probe for *circ-CTNNB1* (arrowheads), with or without treatment using DDX3 antibody or competition using an excess of unlabeled homologous circRNA probe. Student *t* test compared the difference in **G**. *, $P < 0.01$ vs. IgG. $^{\Delta}$, $P < 0.01$ vs. mock.

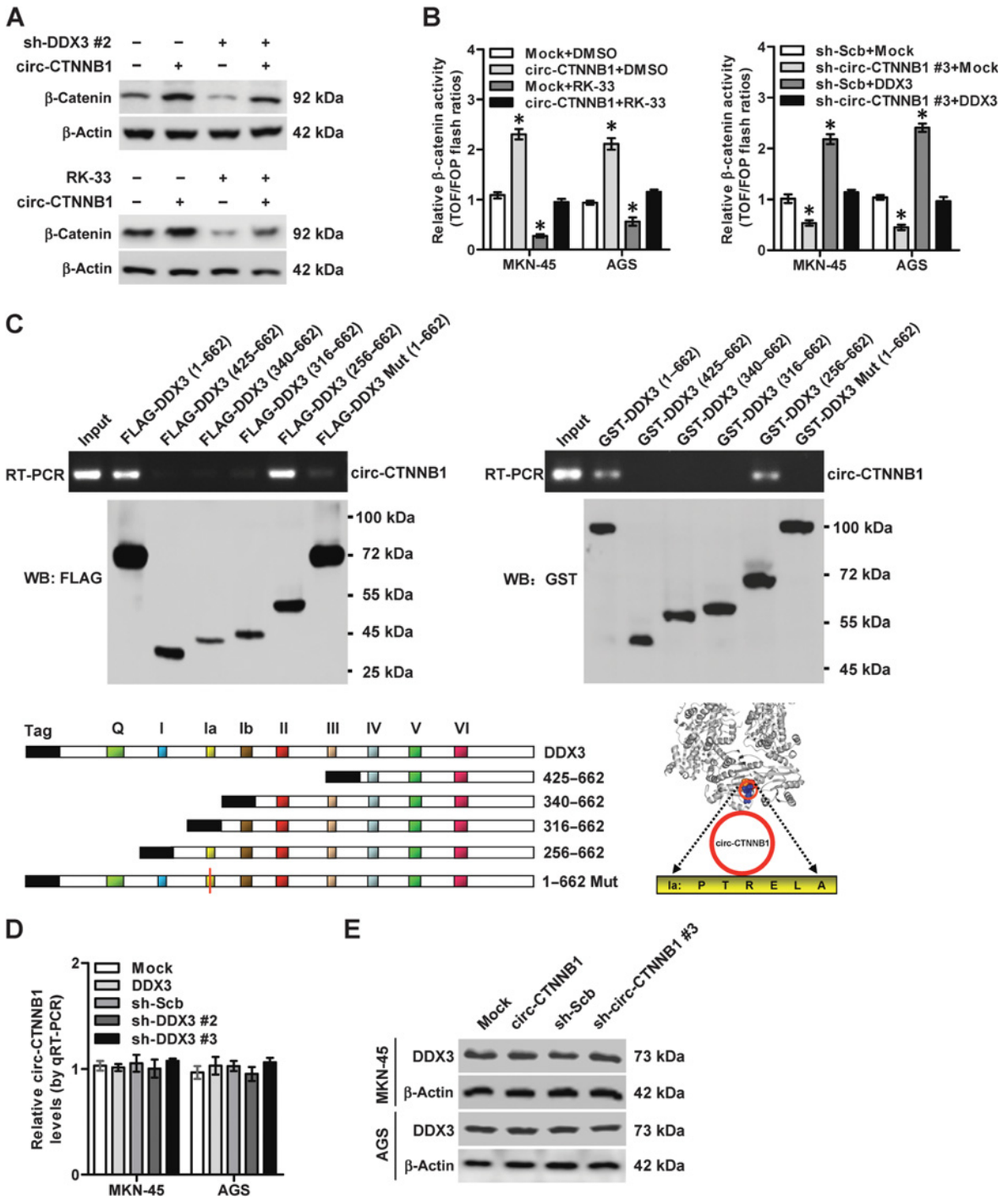

Figure 5.

Circ-CTNNB1 cooperates with DDX3 to facilitate the expression and activity of β-catenin. **A,** Western blot assay showing the expression of β-catenin in MKN-45 cells stably transfected with empty vector (mock) or *circ-CTNNB1* and those cotransfected with sh-DDX3 #2 or treated with a DDX3 inhibitor (RK-33, 5.0 μmol/L). **B,** TOP/FOP flash assay indicating the β-catenin activity in MKN-45 and AGS cells stably transfected with mock, *circ-CTNNB1*, sh-Scb, or sh-circ-CTNNB1 #3, and those treated with RK-33 (5.0 μmol/L) or cotransfected with *DDX3*. **C,** *In vitro* binding assay depicting the recovered *circ-CTNNB1* levels detected by RT-PCR (top) after incubation with full-length, truncation, or mutation (Mut) forms of FLAG-tagged or GST-tagged recombinant DDX3 protein (bottom left) validated by Western blot (middle), with mutation of amino acids (PTRELA) within Ia domain as indicated (bottom right). **D,** Real-time qRT-RCR assay indicating the levels of *circ-CTNNB1* in MKN-45 and AGS cells transfected with mock, *DDX3*, sh-Scb, or sh-DDX3. **E,** Western blot assay showing the expression of DDX3 in MKN-45 and AGS cells transfected with mock, *circ-CTNNB1*, sh-Scb, or sh-circ-CTNNB1 #3. Student *t* test for analyzing the difference in **B** and **D**. *, $P < 0.01$ vs. mock + DMSO or sh-Scb + mock.

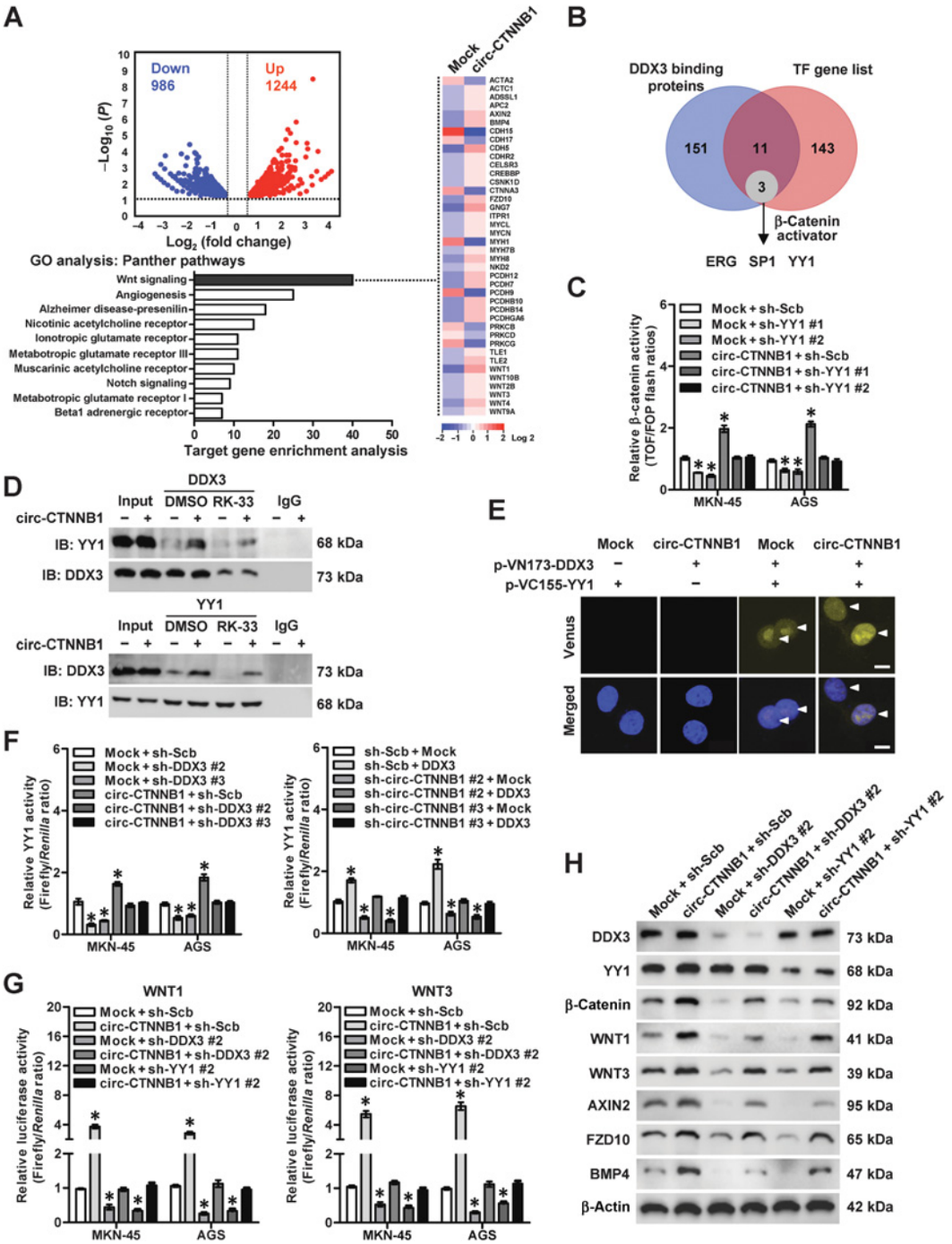

Figure 6.

Circ-CTNNB1 facilitates DDX3-mediated transactivation of YY1 and target gene expression. **A,** Volcano plots (top left) showing the differentially expressed genes (fold change > 1.5, $P < 0.05$) in AGS cells stably transfected with empty vector (mock) or *circ-CTNNB1.* Gene ontology (GO) analysis with PANTHER classification system (http://www.pantherdb.org/) indicating the involved pathway of target genes (bottom left), and heat map showing the differentially expressed genes of the Wnt/β-catenin signaling pathway (right). **B,** Venn diagram indicating the discovery of transcriptional regulators essential for altered genes using DDX3-interacting proteins from the BioGRID database and transcription factor (TF) list from ChIP-X program. **C,** TOP/FOP flash assay showing the β-catenin activity in cancer cells stably transfected with mock or *circ-CTNNB1* and those cotransfected with sh-Scb or sh-YY1. **D,** Coimmunoprecipitation and Western blot assays indicating the interaction between DDX3 and YY1 in MKN-45 cells stably transfected with mock or *circ-CTNNB1* and those treated with DMSO or RK-33 (5.0 μmol/L). **E,** BiFC assay showing the interaction between DDX3 and YY1 in MKN-45 cells stably transfected with mock or *circ-CTNNB1*. **F,** Dual-luciferase assay revealing the transactivation of YY1 in MKN-45 and AGS cells stably transfected with mock, *circ-CTNNB1*, or *DDX3*, and those cotransfected with sh-Scb, sh-DDX3, or sh-circ-CTNNB1. **G,** Dual-luciferase assay indicating the promoter activity of *WNT1* and *WNT3* in MKN-45 and AGS cells stably transfected with mock or *circ-CTNNB1*, and those cotransfected with sh-Scb, sh-DDX3 #2, or sh-YY1 #2. **H,** Western blot assay showing the expression of DDX3, YY1, β-catenin, WNT1, WNT3, AXIN2, FZD10, and BMP4 in MKN-45 cells stably transfected with mock or *circ-CTNNB1*, and those cotransfected with sh-Scb, sh-DDX3 #2, or sh-YY1 #2. Student *t* test for analyzing the difference in **C**, **F**, and **G**. *, $P < 0.01$ vs. mock + sh-Scb.

binding to EZH2 or HDAC1 in MKN-45 cells, which was rescued by knockdown of *DDX3* (Supplementary Fig. S4C). Stable overexpression of *circ-CTNNB1* led to increased binding of YY1 and p300 to the promoters of target genes *WNT1* and *WNT3*, accompanied by decreased recruitment of EZH2 or HDAC1, which were prevented by silencing of *DDX3* (Supplementary Fig. S5A). Consistently, ectopic expression of *circ-CTNNB1* increased the promoter activity of *WNT1* or *WNT3* in MKN-45 and AGS cells, which was abolished by knockdown of *DDX3* or *YY1* (Fig. 6G). The expression of *WNT1*, *WNT3*, *AXIN2*, *FZD10*, and *BMP4* was increased in cancer cells stably transfected with *circ-CTNNB1*, which was suppressed by knockdown of *DDX3* or *YY1* (Fig. 6H; Supplementary Fig. S5B and S5C). Notably, higher levels of *DDX3* ($P < 1.0 \times 10^{-4}$) or *YY1* ($P < 1.0 \times 10^{-4}$) were observed in 81 primary gastric cancer tissues than their paired adjacent normal tissues, especially in specimens with metastasis ($P = 0.023$ and $P < 1.0 \times 10^{-4}$; Supplementary Fig. S6A). Kaplan–Meier survival analysis of this cohort and well-defined gastric cancer cases derived from Kaplan–Meier plotter (http://kmplot.com/analysis) revealed that patients with higher expression of *DDX3* ($P < 1.0 \times 10^{-4}$ and $P = 8.0 \times 10^{-6}$), *YY1* ($P < 1.0 \times 10^{-4}$ and $P = 1.0 \times 10^{-4}$), *WNT1* ($P = 1.0 \times 10^{-11}$), *WNT3* ($P = 2.5 \times 10^{-11}$), *AXIN2* ($P = 3.0 \times 10^{-4}$), *FZD10* ($P = 7.2 \times 10^{-5}$), or *BMP4* ($P = 1.7 \times 10^{-4}$) had lower overall survival probability (Supplementary Fig. S6B and S6C). These results showed that *circ-CTNNB1* facilitated DDX3-mediated transactivation of YY1 and target gene expression in cancer cells.

Therapeutic effects of lentivirus-mediated *circ-CTNNB1* knockdown

We further explored the therapeutic efficiencies of *circ-CTNNB1* knockdown on tumor growth and survival of athymic nude mice bearing xenografts. Knockdown of *circ-CTNNB1* significantly reduced the growth, tumor weight, Ki-67 proliferation index, CD31-positive intratumoral microvessels, and intratumoral expression of *CTNNB1* and downstream genes of AGS cell–formed subcutaneous xenografts (Supplementary Fig. S7A–S7D). In addition, administration of lentivirus-mediated sh-circ-CTNNB1 #3 significantly decreased the lung metastatic colonies and prolonged the survival time of nude mice treated with tail-vein injection of AGS cells (Supplementary Fig. S7E). These results suggested that lentivirus-mediated knockdown of *circ-CTNNB1* suppressed the tumorigenesis and aggressiveness.

Therapeutic peptide blocking the *circ-CTNNB1*–DDX3 interaction

Based on the importance of RNA-binding domain Ia (274–279 aa) of DDX3 in interacting with *circ-CTNNB1*, we further designed a cell-penetrating peptide, named as DDX3 inhibitory peptide with 13 amino acids in length (DIP-13), that might potentially block the *circ-CTNNB1*–DDX3 interaction. Biotin-labeled peptide pulldown assay revealed the binding of DIP-13 to *circ-CTNNB1* (Supplementary Fig. S8A). Administration of DIP-13 resulted in its obvious aggregation within the nucleus (Fig. 7A), abolished the *circ-CTNNB1*–DDX3 interaction (Fig. 7B), and prevented the transactivation of YY1 induced by stable overexpression of *circ-CTNNB1* in cancer cells (Supplementary Fig. S8B). Administration of DIP-13 suppressed the viability of MKN-45 and AGS cells in a dose- and time-dependent manner (Supplementary Fig. S8C). In soft-agar and Matrigel invasion assays, the growth and invasion of viable cancer cells were significantly inhibited by DIP-13 treatment (Fig. 7C and D; Supplementary Fig. S8D–S8E). Intratumoral administration of DIP-13 significantly reduced the volume, tumor weight, Ki-67 proliferation index, and CD31-positive microvessels, and downstream gene expression of subcutaneous xenografts formed by injection of AGS cells (Fig. 7E and F; Supplementary Fig. S8F). In experimental metastasis assay, administration of DIP-13 via the tail vein significantly reduced the lung metastatic colonies and prolonged the survival time of athymic nude mice treated with tail-vein injection of AGS cells (Fig. 7G). Collectively, these results indicated that inhibitory peptide blocking the *circ-CTNNB1*–DDX3 interaction suppressed the growth and aggressiveness of cancer cells.

Discussion

Recent studies show that circRNAs exert functions in multiply ways, such as binding to proteins or possessing protein-coding abilities (6, 12, 31). For example, *circ-Foxo3* induces cell apoptosis through interacting with mouse double minute 2 homolog and increasing p53 stability (32). In this study, we discover that *cis*-acting *circ-CTNNB1* is upregulated in cancer tissues and associated with unfavorable outcome of patients. The action mode of *circ-CTNNB1* is different from previously reported intronic or exon–intron circRNAs (11, 12). *Circ-CTNNB1* does not affect the transcription of *CTNNB1* in cancer cells. Instead, *circ-CTNNB1* is able to activate Wnt signaling and increase the levels of β-catenin protein. Mechanistically, *circ-CTNNB1* interacts with DDX3 to increase the transactivation of YY1, which regulates the expression of genes associated with β-catenin activation and cancer progression (Fig. 7H), such as *WNT1* (33), *WNT3* (34), *AXIN2* (35), *FZD10* (36), and *BMP4* (37). Our evidence demonstrates that *circ-CTNNB1* possesses oncogenic properties to drive cancer progression, representing a promising therapeutic target for cancers.

DDX3, a member of the DEAD-box RNA helicase family, plays multiple roles in RNA metabolism, such as transcription, pre-mRNA splicing, and mRNA export (38). High *DDX3* expression is associated with tumor progression and poor prognosis in breast cancer and gallbladder cancer (38). In glioblastoma, DDX3 facilitates the motility of cancer cells by increasing Snail expression (39). Meanwhile, DDX3 promotes the migration and invasion of colorectal cancer cells via the Snail/E-cadherin pathway (40). On the contrary, downregulation of *DDX3* is associated with poor prognosis in hepatocellular carcinoma (41) and lung cancer (42). These findings indicate that *DDX3* exerts oncogenic or tumor-suppressive functions in a context-dependent manner. In the current study, we demonstrated that *DDX3* was associated with poor outcome of patients with gastric cancer. Gain- and loss-of-function studies indicated that DDX3 facilitated the β-catenin activity of cancer cells, suggesting the oncogenic roles of *DDX3* in cancer progression.

As a transcriptional regulator, DDX3 has been reported to regulate the promoter activity of *p21* (43) and *E-cadherin* (44). DDX3 also acts as a cofactor for transcription factor SP1 to synergistically activate the transcription of oncogenic *KRAS* (45). In addition, DDX3 promotes the stabilization and nuclear accumulation of p53 (46). Recent studies reveal that DDX3 is able to activate Wnt signaling through binding with casein kinase 1 to stimulate its kinase activity (47), or interacting with 5′-untranslated region of Rac family small GTPase 1 to facilitate its translation (48). However, the roles of noncoding RNA in regulating the DDX3 activity in cancer progression remain to be determined.

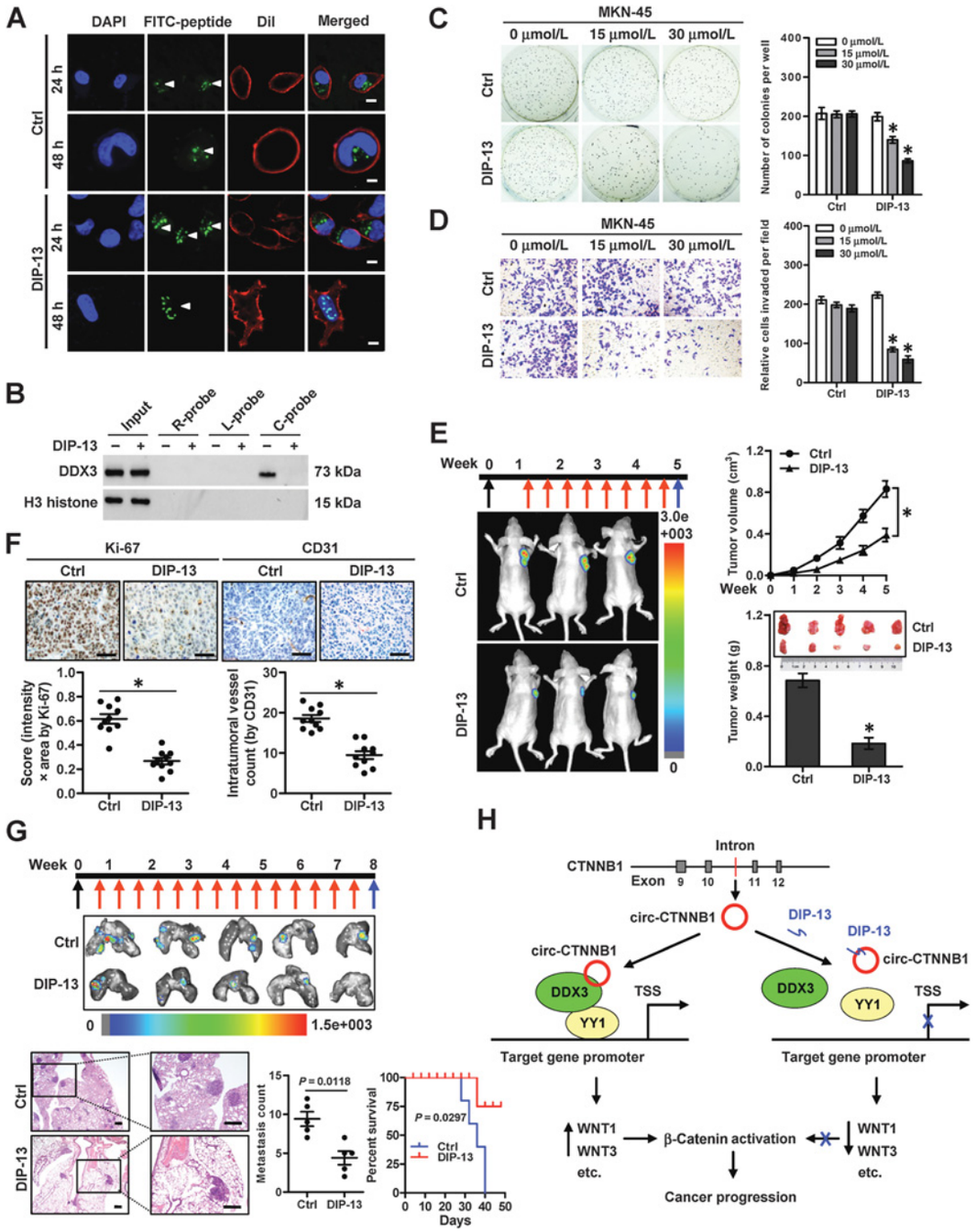

Figure 7.

Therapeutic peptide blocking the *circ-CTNNB1*–DDX3 interaction. **A,** Confocal images showing the distribution of FITC-labeled control (Ctrl) or inhibitory (DIP-13) peptide (30 μmol/L) within MKN-45 cells, with nuclei and cellular membrane stained with DAPI (blue) or DiI (red), respectively. Scale bars, 10 μm. **B,** Western blot indicating the DDX3 protein pulled down by biotin-labeled random (R), linear (L), or circular (C) *circ-CTNNB1* probe from the lysates of MKN-45 cells treated with Ctrl peptide or DIP-13 (30 μmol/L). **C** and **D,** Representative images (left) and quantification (right) of soft-agar (**C**) and Matrigel invasion (**D**) assays showing the anchorage-independent growth and invasion capability of viable MKN-45 cells treated with Ctrl peptide or DIP-13 (30 μmol/L) for 24 hours. **E,** Representative images (left), *in vivo* growth curve (top right), and tumor weight at the end points (bottom right) of AGS cell-formed subcutaneous xenografts in nude mice ($n = 5$ for each group) that were treated with intratumoral injection of Ctrl peptide or DIP-13 (3 mg/kg) as indicated (left). **F,** Representative images (top) and quantification (bottom) of IHC staining indicating the expression of Ki-67 and CD31 in xenografts treated with intratumoral injection of Ctrl peptide or DIP-13 (3 mg/kg). **G,** Representative images (top), hematoxylin and eosin staining (bottom left) and quantification (bottom middle) of lung metastatic colonization, and Kaplan–Meier curves (bottom right) of nude mice ($n = 5$ for each group) treated with tail-vein injection of AGS cells and subsequent administration of Ctrl peptide or DIP-13 (3 mg/kg) as indicated. **H,** The mechanisms underlying *circ-CTNNB1*–promoted cancer progression. As a *cis*-acting circRNA, *circ-CTNNB1* binds DDX3 to facilitate its interaction with YY1, resulting in transactivation of YY1 and transcriptional alteration of target genes associated with β-catenin activation and cancer progression. An inhibitory peptide DIP-13 is able to block the *circ-CTNNB1*–DDX3 interaction and suppress cancer progression. Student *t* test and analysis of variance analyzed the difference in **C–G**. Log-rank test for survival comparison in **G**. *, $P < 0.01$ vs. Ctrl.

In this study, we demonstrate that DDX3 functions as a cofactor to facilitate the transactivation of YY1. As a transcription factor, YY1 is upregulated in many types of cancers and exerts its oncogenic effects through initiating, activating, or repressing the transcription of target genes (49). Notably, we found that the electrophoresis speed of N-terminus (1–200 amino acids) of YY1 protein was slower than that of C-terminus (201–414 amino acids), which was in line with previous findings that special structure affects its electrophoresis speed (50). Our results indicate that *circ-CTNNB1* binds the Ia domain of DDX3 protein to increase its interaction with YY1, resulting in transactivation of YY1. We believe that the binding of *circ-CTNNB1* might result in altered DDX3 protein structure that facilitates its interaction with YY1, with the underlying mechanisms warranting further investigation. Because inhibition of *circ-CTNNB1*–DDX3 interaction abolishes the aggressive behavior of cancer cells, our findings indicate that the tumor promoting functions of *circ-CTNNB1* are mediated, at least in part, through interacting with DDX3.

In summary, for the first time, we have demonstrated that *circ-CTNNB1* is upregulated in cancer tissues and associated with poor outcome of patients with gastric cancer. *Circ-CTNNB1* cooperates with DDX3 to promote the tumorigenesis and aggressiveness of cancer cells through facilitating transactivation of YY1 and transcriptional alteration of target genes associated with β-catenin activation and cancer progression. Administration of lentivirus-mediated shRNA targeting *circ-CTNNB1* or a cell-penetrating inhibitory peptide blocking the *circ-CTNNB1*–DDX3 interaction suppresses the growth and aggressiveness of cancer cells. This study extends our knowledge about the regulation of Wnt/β-catenin signaling by *cis*-acting circRNA and suggests that *circ-CTNNB1* and *DDX3* may be potential therapeutic targets for human cancers. Meanwhile, the roles of other *trans*-acting circRNA in β-catenin activation and cancer progression warrant further investigation.

Disclosure of Potential Conflicts of Interest

No potential conflicts of interest were disclosed.

Authors' Contributions

Conception and design: L. Zheng, Q. Tong
Development of methodology: F. Yang, E. Fang, D. Li
Acquisition of data (provided animals, acquired and managed patients, provided facilities, etc.): F. Yang, E. Fang, H. Mei, Y. Chen, H. Li, D. Li, H. Song, J. Wang, M. Hong, W. Xiao, X. Wang
Analysis and interpretation of data (e.g., statistical analysis, biostatistics, computational analysis): F. Yang, K. Huang, L. Zheng, Q. Tong
Writing, review, and/or revision of the manuscript: L. Zheng, Q. Tong
Administrative, technical, or material support (i.e., reporting or organizing data, constructing databases): D. Li, X. Wang, K. Huang
Study supervision: L. Zheng, Q. Tong

Acknowledgments

We appreciate Drs. Christof Niehrs and Makoto Miyagishi for providing vectors. This work was supported by the National Natural Science Foundation of China (81272779, 81472363, 81402301, 81672500, 81772967, 81874085 to Q. Tong; 81372667, 81572423, 81874066 to L. Zheng; 81402408, 81773094 to H. Mei; 81802925 to D. Li).

The costs of publication of this article were defrayed in part by the payment of page charges. This article must therefore be hereby marked *advertisement* in accordance with 18 U.S.C. Section 1734 solely to indicate this fact.

Received May 20, 2018; revised September 27, 2018; accepted December 11, 2018; published first December 18, 2018.

References

1. Logan CY, Nusse R. The Wnt signaling pathway in development and disease. Annu Rev Cell Dev Biol 2004;20:781–810.
2. van de Wetering M, Sancho E, Verweij C, de Lau W, Oving I, Hurlstone A, et al. The beta-catenin/TCF-4 complex imposes a crypt progenitor phenotype on colorectal cancer cells. Cell 2002;111:241–50.
3. Mir R, Pradhan SJ, Patil P, Mulherkar R, Galande S. Wnt/β-catenin signaling regulated SATB1 promotes colorectal cancer tumorigenesis and progression. Oncogene 2015;35:1679–91.
4. Zhang K, Guo Y, Wang X, Zhao H, Ji Z, Cheng C, et al. WNT/β-catenin directs self-renewal symmetric cell division of hTERThigh prostate cancer stem cells. Cancer Res 2017;77:2534–47.
5. Jeck WR, Sharpless NE. Detecting and characterizing circular RNAs. Nat Biotechnol 2014;32:453–61.
6. Li Y, Zheng Q, Bao C, Li S, Guo W, Zhao J, et al. Circular RNA is enriched and stable in exosomes: a promising biomarker for cancer diagnosis. Cell Res 2015;25:981–4.
7. Memczak S, Jens M, Elefsinioti A, Torti F, Krueger J, Rybak A, et al. Circular RNAs are a large class of animal RNAs with regulatory potency. Nature 2013;495:333–8.
8. Hansen TB, Jensen TI, Clausen BH, Bramsen JB, Finsen B, Damgaard CK, et al. Natural RNA circles function as efficient microRNA sponges. Nature 2013;495:384–8.
9. Ashwal-Fluss R, Meyer M, Pamudurti Nagarjuna R, Ivanov A, Bartok O, Hanan M, et al. circRNA biogenesis competes with pre-mRNA splicing. Mol Cell 2014;56:55–66.
10. Abdelmohsen K, Panda AC, Munk R, Grammatikakis I, Dudekula DB, De S, et al. Identification of HuR target circular RNAs uncovers suppression of PABPN1 translation by circPABPN1. RNA Biol 2017;14:361–9.
11. Zhang Y, Zhang XO, Chen T, Xiang JF, Yin QF, Xing YH, et al. Circular intronic long noncoding RNAs. Mol Cell 2013;51:792–806.
12. Li Z, Huang C, Bao C, Chen L, Lin M, Wang X, et al. Exon–intron circular RNAs regulate transcription in the nucleus. Nat Struct Mol Biol 2015;22:256–64.
13. Huang G, Li S, Yang N, Zou Y, Zheng D, Xiao T. Recent progress in circular RNAs in human cancers. Cancer Lett 2017;404:8–18.
14. Cadigan KM, Waterman ML. TCF/LEFs and Wnt signaling in the nucleus. Cold Spring Harb Perspect Biol 2012;4:a007906.
15. Li D, Wang X, Mei H, Fang E, Ye L, Song H, et al. Long noncoding RNA pancEts-1 promotes neuroblastoma progression through hnRNPK-mediated β-catenin stabilization. Cancer Res 2018;78:1169–83.
16. Zhao X, Li D, Pu J, Mei H, Yang D, Xiang X, et al. CTCF cooperates with noncoding RNA MYCNOS to promote neuroblastoma progression through facilitating MYCN expression. Oncogene 2016;35:3565–76.
17. Petkovic S, Muller S. RNA circularization strategies *in vivo* and *in vitro*. Nucleic Acids Res 2015;43:2454–65.
18. Chen C, Sarnow P. Initiation of protein synthesis by the eukaryotic translational apparatus on circular RNAs. Science 1995;268:415–7.
19. Glažar P, Papavasileiou P, Rajewsky N. circBase: a database for circular RNAs. RNA 2014;20:1666–70.
20. Dudekula DB, Panda AC, Grammatikakis I, De S, Abdelmohsen K, Gorospe M. CircInteractome: A web tool for exploring circular RNAs and their interacting proteins and microRNAs. RNA Biol 2016;13:34–42.
21. Tang X, Zheng D, Hu P, Zeng Z, Li M, Tucker L, et al. Glycogen synthase kinase 3 beta inhibits microRNA-183–96-182 cluster via the β-Catenin/TCF/LEF-1 pathway in gastric cancer cells. Nucleic Acids Res 2014;42:2988–98.
22. Afifi MM, Austin LA, Mackey MA, El-Sayed MA. XAV939:From a small inhibitor to a potent drug bioconjugate when delivered by gold nanoparticles. Bioconjug Chem 2014;25:207–15.
23. Xie M, Vesuna F, Tantravedi S, Bol GM, Heerma van Voss MR, Nugent K, et al. RK-33 radiosensitizes prostate cancer cells by blocking the RNA helicase DDX3. Cancer Res 2016;76:6340–50.

24. Walia RR, Xue LC, Wilkins K, El-Manzalawy Y, Dobbs D, Honavar V. RNABindRPlus: a predictor that combines machine learning and sequence homology-based methods to improve the reliability of predicted RNA-binding residues in proteins. PLoS One 2014;9:e97725.
25. Lachmann A, Xu H, Krishnan J, Berger SI, Mazloom AR, Ma'ayan A. ChEA: transcription factor regulation inferred from integrating genome-wide ChIP-X experiments. Bioinformatics 2010;26:2438–44.
26. Chatr-aryamontri A, Oughtred R, Boucher L, Rust J, Chang C, Kolas NK, et al. The BioGRID interaction database: 2017 update. Nucleic Acids Res 2017;45:D369–D379.
27. Wu L, Zhao JC, Kim J, Jin HJ, Wang CY, Yu J. ERG is a critical regulator of Wnt/LEF1 signaling in prostate cancer. Cancer Res 2013;73: 6068–79.
28. Kwon YJ, Baek HS, Ye DJ, Shin S, Kim D, Chun YJ. CYP1B1 enhances cell proliferation and metastasis through induction of EMT and activation of Wnt/beta-catenin signaling via Sp1 upregulation. PLoS One 2016;11: e0151598.
29. Lu C, Thoeni C, Connor A, Kawabe H, Gallinger S, Rotin D. Intestinal knockout of Nedd4 enhances growth of Apc(min) tumors. Oncogene 2016;35:5839–49.
30. Hu CD, Kerppola TK. Simultaneous visualization of multiple protein interactions in living cells using multicolor fluorescence complementation analysis. Nat Biotechnol 2003;21:539–45.
31. Du WW, Yang W, Liu E, Yang Z, Dhaliwal P, Yang BB. Foxo3 circular RNA retards cell cycle progression via forming ternary complexes with p21 and CDK2. Nucleic Acids Res 2016;44:2846–58.
32. Du WW, Fang L, Yang W, Wu N, Awan FM, Yang Z, et al. Induction of tumor apoptosis through a circular RNA enhancing Foxo3 activity. Cell Death Differ 2017;24:357–70.
33. Zhang JG, Shi Y, Hong DF, Song M, Huang D, Wang CY, et al. MiR-148b suppresses cell proliferation and invasion in hepatocellular carcinoma by targeting WNT1/β-catenin pathway. Sci Rep 2015;5:8087.
34. Wu Y, Ginther C, Kim J, Mosher N, Chung S, Slamon D, et al. Expression of Wnt3 activates Wnt/β-catenin pathway and promotes EMT-like phenotype in trastuzumab resistant HER2-overexpressing breast cancer cells. Mol Cancer Res 2012;10:1597–606.
35. Li Y, Jin K, van Pelt GW, van Dam H, Yu X, Mesker WE, et al. c-Myb enhances breast cancer invasion and metastasis through the Wnt/β-catenin/axin2 pathway. Cancer Res 2016;76:3364–75.
36. Gong C, Qu S, Lv XB, Liu B, Tan W, Nie Y, et al. BRMS1L suppresses breast cancer metastasis by inducing epigenetic silence of FZD10. Nat Commun 2014;5:5406.
37. Kim JS, Crooks H, Dracheva T, Nishanian TG, Singh B, Jen J, et al. Oncogenic beta-catenin is required for bone morphogenetic protein 4 expression in human cancer cells. Cancer Res 2002;62: 2744–8.
38. Bol GM, Xie M, Raman V. DDX3, a potential target for cancer treatment. Mol Cancer 2015;14:188.
39. Sun M, Song L, Zhou T, Gillespie GY, Jope RS. The role of DDX3 in regulating snail. Biochim Biophys Acta 2011;1813:438–47.
40. Su CY, Lin TC, Lin YF, Chen MH, Lee CH, Wang HY, et al. DDX3 as a strongest prognosis marker and its downregulation promotes metastasis in colorectal cancer. Oncotarget 2015;6:18602–12.
41. Zhang H, Xing Z, Mani SK, Bancel B, Durantel D, Zoulim F, et al. RNA helicase DEAD box protein 5 regulates polycomb repressive complex 2/Hox transcript antisense intergenic RNA function in hepatitis B virus infection and hepatocarcinogenesis. Hepatology 2016;64: 1033–48.
42. Wu DW, Liu WS, Wang J, Chen CY, Cheng YW, Lee H. Reduced p21(WAF1/CIP1) via alteration of p53-DDX3 pathway is associated with poor relapse-free survival in early-stage human papillomavirus-associated lung cancer. Clin Cancer Res 2011;17:1895–905.
43. Chao CH, Chen CM, Cheng PL, Shih JW, Tsou AP, Lee YH. DDX3, a DEAD box RNA helicase with tumor growth-suppressive property and transcriptional regulation activity of the p21waf1/cip1 promoter, is a candidate tumor suppressor. Cancer Res 2006;66:6579–88.
44. Botlagunta M, Vesuna F, Mironchik Y, Raman A, Lisok A, Winnard P, et al. Oncogenic role of DDX3 in breast cancer biogenesis. Oncogene 2008;27:3912–22.
45. Wu DW, Lin PL, Cheng YW, Huang CC, Wang L, Lee H. DDX3 enhances oncogenic KRAS induced tumor invasion in colorectal cancer via the betacatenin/ZEB1 axis. Oncotarget 2016;7:22687–99.
46. Sun M, Zhou T, Jonasch E, Jope RS. DDX3 regulates DNA damage-induced apoptosis and p53 stabilization. Biochim Biophys Acta 2013;1833: 1489–97.
47. Cruciat CM, Dolde C, de Groot RE, Ohkawara B, Reinhard C, Korswagen HC, et al. RNA helicase DDX3 is a regulatory subunit of casein kinase 1 in Wnt-beta-catenin signaling. Science 2013;339:1436–41.
48. Chen HH, Yu HI, Cho WC, Tarn WY. DDX3 modulates cell adhesion and motility and cancer cell metastasis via Rac1-mediated signaling pathway. Oncogene 2015;34:2790–800.
49. Shi J, Hao A, Zhang Q, Sui G. The role of YY1 in oncogenesis and its potential as a drug target in cancer therapies. Curr Cancer Drug Targets 2015;15:145–57.
50. Lorente M, Pérez C, Sánchez C, Donohoe M, Shi Y, Vidal M. Homeotic transformations of the axial skeleton of YY1 mutant mice and genetic interaction with the polycomb group gene Ring1/Ring1A. Mech Dev 2006;123:312–20.